JOURNAL OF GEOPHYSICAL RESEARCH: ATMOSPHERES, VOL. 118, 1459–1470, doi:10.1002/jgrd.50133, 2013

Air-mass origin as a diagnostic of tropospheric transport

Clara Orbe,[1] Mark Holzer,[1,2] Lorenzo M. Polvani,[1,3] and Darryn Waugh[4]

Received 9 May 2012; revised 2 October 2012; accepted 20 December 2012; published 7 February 2013.

[1] We introduce rigorously defined air masses as a diagnostic of tropospheric transport. The fractional contribution from each air mass partitions air at any given point according to either where it was last in the planetary boundary layer or where it was last in contact with the stratosphere. The utility of these air-mass fractions is demonstrated for the climate of a dynamical core circulation model and its response to specified heating. For an idealized warming typical of end-of-century projections, changes in air-mass fractions are in the order of 10% and reveal the model's climate change in tropospheric transport: poleward-shifted jets and surface-intensified eddy kinetic energy lead to more efficient stirring of air out of the midlatitude boundary layer, suggesting that, in the future, there may be increased transport of black carbon and industrial pollutants to the Arctic upper troposphere. Correspondingly, air is less efficiently mixed away from the subtropical boundary layer. The air-mass fraction that had last stratosphere contact at midlatitudes increases all the way to the surface, in part due to increased isentropic eddy transport across the tropopause. Correspondingly, the air-mass fraction that had last stratosphere contact at high latitudes is reduced through decreased downwelling across the tropopause. A weakened Hadley circulation leads to decreased interhemispheric transport in the model's future climate.

Citation: Orbe, C., M. Holzer, L. M. Polvani, and D. Waugh (2013), Air-mass origin as a diagnostic of tropospheric transport, *J. Geophys. Res. Atmos.*, *118*, 1459–1470, doi:10.1002/jgrd.50133.

1. Introduction

[2] Global warming is expected to lead to poleward shifting, strengthening tropospheric jets, and a weakened Hadley circulation [e.g., *Yin*, 2005; *Miller et al.*, 2006]. Because the tropospheric jets (the associated baroclinic eddies) and the meridional overturning circulation are all keys to controlling the transport of energy and momentum, the question arises: What are the quantitative effects of these circulation changes on tropospheric constituent transport? The climate change signature on basic state variables such as temperature, humidity, winds, and chemical composition, particularly in the ozone, has been analyzed in a vast number of studies and continues to be of great interest. In comparison, the signature of climate change on large-scale tropospheric transport has received relatively little attention despite its importance for understanding changes in composition and global air quality, which are not only driven by changes in chemistry and emissions but also by crucial changes in atmospheric flow.

[3] Here, we will use an idealized atmospheric circulation model to demonstrate how changes in tropospheric transport can be quantified in a tracer-independent manner by using synthetic Green function tracers that quantify a fundamental aspect of the atmosphere's advective-eddy-diffusive transport operator, which is independent of any particular trace species. Although *Holzer and Boer* [2001] explored the issue in terms of timescales and the large-scale structure of tracers with specified idealized emissions, our focus here is on the spatial distribution of rigorously defined air masses, which are a particularly simple tracer-independent transport diagnostic ideally suited to model investigations of climate change. Because anthropogenic and biogenic trace species originate primarily in the planetary boundary layer (PBL), and the stratosphere is a source of ozone and cosmogenic tracers for the troposphere, we define both PBL and stratospheric (STRAT) air-mass fractions. More precisely, the PBL air-mass fraction at a point $\mathbf{r}$, whose surface origin was geographic region Ω_i, is simply defined as the mass fraction of the air at $\mathbf{r}$ that had its last contact with the PBL in region Ω_i. An air-mass fraction can be thought of as a label of where last PBL contact occurred, allowing an assessment of the relative importance of different source regions. STRAT air-mass fractions are defined analogously.

[4] Air-mass fractions thus defined are the atmospheric equivalent of water-mass fractions, which have a long history of being used in oceanography [e.g., *Tomczak*, 1981; *Haine and Hall*, 2002; *Holzer et al.*, 2010], but have not yet been adopted by the atmospheric science community. Air-mass fractions can be computed in any atmospheric

[1]Department of Applied Physics and Applied Mathematics, Columbia University, New York, New York, USA.
[2]Department of Applied Mathematics, School of Mathematics and Statistics, University of New South Wales, Sydney, New South Wales, Australia.
[3]Department of Earth and Environmental Sciences, Columbia University, New York, New York, USA.
[4]Department of Earth and Planetary Sciences, Johns Hopkins University, Baltimore, Maryland, USA.

Corresponding author: C. Orbe, Department of Applied Physics and Applied Mathematics, Columbia University, New York, NY 10027, USA. (co2203@columbia.edu).

2169-897X/13/10.1002/jgrd.50133

transport model as simple equilibrated tracer mixing ratios with appropriate boundary conditions. The air-mass fractions show where, and with what dilution, air from various source regions can be found. Air-mass fractions, and their changes, thus help to isolate the role of transport from that of chemistry and changing emissions in shaping the atmosphere's changing chemical composition. Here, we use a relatively simple, idealized model of the atmosphere to demonstrate the utility of air-mass fractions as a first-order tracer-independent diagnostic of tropospheric transport and its climate change.

[5] The statistical properties of transport can usefully be referred to as "transport climate" [*Holzer and Boer*, 2001]. In this paper, we quantify the change in transport climate with idealized warming by examining the difference in the climatological mean air-mass fractions between two time slice integrations with a "dynamical core" circulation model [*Wang et al*., 2012]: one for idealized current conditions and another for idealized future conditions with a specified heating in the upper tropical troposphere.

[6] We emphasize that it is our goal to demonstrate the use of air-mass fractions as a diagnostic of changes in the transport climate—it is not our aim to make detailed, high-fidelity projections of how atmospheric transport is likely to change in the future. The climate of the dynamical core circulation, and its change with prescribed heating, are ideal for this purpose because they avoid the complexities of comprehensive climate models while still capturing key dynamic large-scale changes as demonstrated by *Wang et al*. [2012].

[7] Broadly, the changes in the air-mass fractions are on the order of 10% with patterns that are interpretable in terms of changes in the mean flow and in the eddy statistics. However, unlike the flow statistics, the air-mass fractions quantify the integrated effect of advection and eddy diffusion along all possible paths from their region of origin to the point of interest.

2. Theory of Air-Mass Fractions

[8] For definiteness, consider the air-mass fractions that label PBL origin. In order to identify where last PBL contact occurred, we subdivide the entire volume of the Earth's PBL, denoted by Ω, into smaller geographic regions Ω_i (for example, zonal strips of fixed width, as used in later sections). The mass fraction that had last contact with the PBL in region Ω_i, and not elsewhere, is by definition equal to unity in Ω_i and equal to zero in the complement of Ω_i (the rest of Ω), denoted by Ω_i^c. Hence, a passive tracer f, whose mixing ratio is in statistical equilibrium with the boundary conditions of $f = 1$ in Ω_i and $f = 0$ in Ω_i^c, without any other sources or sinks, has the desired interpretation: The corresponding interior mixing ratio at $(\mathbf{r},t)$, denoted by $f(\mathbf{r}, t|\Omega_i)$, is the mass fraction of air that had last contact with the PBL on Ω_i and not elsewhere, that is, the mass fraction whose PBL "region of origin" was Ω_i.

[9] The boundary conditions on f may be thought of as labeling a fluid element (particle) when it is in Ω_i as being 100% Ω_i PBL air, and removing this label (setting it to zero) as soon as the particle finds itself in the PBL somewhere outside of Ω_i. Because the interior volume of Ω cannot be reached without passing through its surface, the labeling and unlabeling may be thought of as occurring on the mathematical surface dividing Ω from the rest of the atmosphere. The mixing ratio $f(\mathbf{r}, t|\Omega_i)$ quantifies the admixture of air with Ω_i labels (ones), and with Ω_i^c labels (zeros), which allows us to interpret f as the desired mass fraction.

[10] With this physical background, f obeys the passive tracer continuity equation without source/sink terms

$$(\partial_t + \mathcal{T})f(\mathbf{r}, t|\Omega_i) = 0 \quad , \tag{1}$$

in the interior of the atmosphere (that is, outside of Ω). In equation (1), $\mathcal{T}$ denotes the linear advection-diffusion transport operator, and for points $\mathbf{r}_\Omega \in \Omega$, the fraction f satisfies the boundary condition

$$f(\mathbf{r}_\Omega, t|\Omega_i) = \Delta(\mathbf{r}_\Omega, \Omega_i) \quad , \tag{2}$$

where $\Delta(\mathbf{r}_\Omega,\Omega_i) = 1$ if $\mathbf{r}_\Omega \in \Omega_i$ and $\Delta(\mathbf{r}_\Omega,\Omega_i) = 0$ if $\mathbf{r}_\Omega \in \Omega_i^c$.

[11] By construction, when equilibrium with the boundary conditions has been reached, the air-mass fractions are precisely normalized so that

$$\sum_{\Omega_i} f(\mathbf{r}, t|\Omega_i) = 1 \quad , \tag{3}$$

at every point $\mathbf{r}$ and time t.

[12] This follows from the fact that the boundary condition (2) ensures that the sum of the fraction is always held at unity over the entire PBL so that, after all initial conditions have decayed, the sum of the fractions must be equal to the boundary value throughout the entire atmosphere. The normalization (3) must hold at all points $\mathbf{r}$ once equilibrium is established. Therefore, equation (3) provides a very useful numerical check for whether equilibrium has been reached.

[13] We note in passing that the air-mass fractions can also straightforwardly be extended to include seasonality, that is, $f(\mathbf{r}, t|\Omega_i) \rightarrow f(\mathbf{r}, t|\Omega_i, \phi)$, where ϕ is the phase of the annual cycle during which last contact with Ω_i occurred. This has been done successfully in the oceanic case [*Holzer et al*., 2010], but we will not do so here for the sake of simplicity, and because we will explore an application of air-mass fractions to idealized climate change with a model run under perpetual boreal winter conditions.

[14] For the STRAT air-mass fractions, our boundary region Ω is conveniently defined to be the entire volume of the stratosphere, which is then subdivided into geographic regions Ω_i. For the idealized circulation model considered here, we choose the Ω_i to be zonally symmetric strips for both the PBL and STRAT cases, which are shown in Figure 1 with a schematic illustration of the corresponding air-mass fractions at a point in the troposphere.

2.1. Connection With Boundary Propagator

[15] The air-mass fractions are also equal to the transit time integrated boundary propagator Green function, $\mathcal{G}(\mathbf{r}, t|\Omega_i, t')$, which propagates mixing ratios specified on the boundary Ω into the interior [e.g., *Holzer and Hall*, 2000; *Haine and Hall*, 2002; *Holzer et al*., 2010]. Although this connection need not be invoked to define, compute, or interpret $f(\mathbf{r}, t|\Omega_i)$, it is nevertheless worthwhile to view the mass fractions in this wider context to connect and contrast them with transit time distributions (TTDs, also called age spectra [*Hall and Plumb*, 1994]). Physically, the boundary propagator $\mathcal{G}(\mathbf{r}, t|\Omega_i, t')dt'$ is the mass fraction of air at $(\mathbf{r},t)$ that had last contact with Ω at subregion Ω_i during $(t', t' + dt')$. Equivalently, $\mathcal{G}(\mathbf{r}, t|\Omega_i, t')$ is the joint probability density distribution at $(\mathbf{r},t)$ of last contact location Ω_i and last contact time t'. The mass fraction f

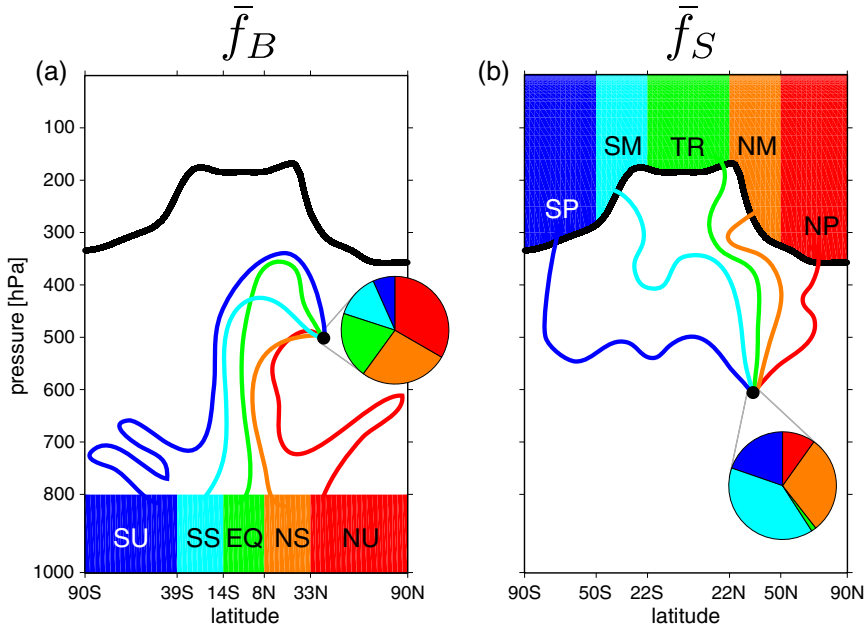

Figure 1. Schematic illustration of the PBL air-mass fractions $\bar{f}_B(\mathbf{r}|\Omega_i)$ and the STRAT air-mass fractions $\bar{f}_S(\mathbf{r}|\Omega_i)$. The heavy black line indicates the tropopause. The air-mass fractions partition air at point $\mathbf{r}$ according to where last contact occurred with (a) the PBL, or (b) the stratosphere. The Ω_i regions are defined as zonal strips indicated by the different colors and identified in the text by their two-letter labels.

is the corresponding marginal distribution with respect to Ω_i (other distributed variables are integrated out), that is,

$$f(\mathbf{r},t|\Omega_i) = \int_{-\infty}^{t} dt' \mathcal{G}\left(\mathbf{r},t|\Omega_i,t'\right) \quad . \tag{4}$$

[16] Likewise, the distribution of transit times since last contact anywhere with Ω is the marginal distribution with respect to t' given by $G\left(\mathbf{r},t|t'\right) = \sum_{\Omega_i} \mathcal{G}\left(\mathbf{r},t|\Omega_i,t'\right)$, with the ideal mean age $\Gamma(\mathbf{r},t) \equiv \int_{-\infty}^{t} dt' \left(t-t'\right) G\left(\mathbf{r},t|t'\right)$. Thus, the TTD and the air-mass fraction summarize complementary aspects of the boundary propagator Green function: the TTD captures the transit time dependence regardless of surface origin, whereas f captures the surface origin dependence regardless of transit time.

3. Experimental Design

3.1. Idealized Circulation and Transport Model

[17] To demonstrate the utility of our diagnostics, we use a model of the dry atmosphere with idealized thermodynamic and momentum forcings as described by *Polvani and Kushner* [2002]. Temperature is linearly restored to a prescribed zonally symmetric reference field that is almost identical to that of the study by *Held and Suarez* [1994], except for a factor to cause hemispherically asymmetric temperature gradients to better capture perpetual December, January, February (DJF) conditions. This Newtonian temperature relaxation drives baroclinic eddies in the troposphere and a polar vortex in the stratosphere through an imposed cold anomaly above 100 hPa in the Northern Hemisphere (NH). Surface friction is modeled as Rayleigh drag. To model realistic stratospheric variability (in terms of frequency of stratospheric sudden warmings and stratosphere-troposphere coupling), we use the configuration of *Gerber and Polvani* [2009]. This configuration sets the polar vortex lapse rate to 4 K/km and imposes 3 km amplitude zonal wave number 2 topography in the NH midlatitudes centered at 45°N.

[18] We approximate the effect of increased greenhouse gas (GHG) concentrations by adding to the reference (REF) configuration a prescribed localized heating centered at approximately 300 hPa on the equator as in *Wang et al.* [2012]. The pattern of the prescribed heating is a zonally symmetric Gaussian with a half-width of approximately 27° in latitude and approximately 25 hPa in pressure, and an amplitude of 0.2 K/d. This pattern was chosen to produce an upper tropical tropospheric warming of approximately 5 K. (The midlatitude surface warms by ~1 K.) This response is broadly similar to end-of-21st-century warming trends under the A1B emissions scenario as predicted by comprehensive general circulation models (GCMs) in the Coupled Model Intercomparison Project, Phase 3 scenario integrations [*Meehl et al.*, 2007]. In the context of our dry model, the warming should be viewed not as a direct heating induced by GHGs but rather as a response of a moist atmosphere to GHG-induced surface warming.

[19] The model integrates the global primitive equations in sigma coordinates using pseudospectral code developed by the Geophysical Fluid Dynamics Laboratory. We run at T42 horizontal resolution with 40 sigma levels, roughly equally spaced in height to 0.01 hPa. The resolution dependence of basic flow diagnostics has been documented by *Wang et al.* [2012]. The sensitivity of the total upward mass flux at 100 hPa is in the order of 10% for a doubling of horizontal resolution, whereas the upward mass flux is insensitive to a doubling of vertical resolution.

[20] Spin-up to a statistically stationary state for the dynamical variables (not the tracers) takes approximately 2000 days for both the REF and future (FTR) configurations. After spin-up, we introduce our diagnostic tracers and integrate them using a Lin-Rood semi-Lagrangian scheme [*Lin and Rood*, 1996] for horizontal advection and a finite-volume parabolic scheme for vertical advection [*Langenhorst*, 2005]. No explicit diffusion is applied to tracers, but for vorticity, divergence, and temperature, the model applies horizontal hyperdiffusion of the form ∇^8.

[21] The model does not include moist convection or seasonal variability nor is the resolution high enough to resolve gravity waves. However, our idealized model contains the key physical elements for capturing the large-scale dynamical changes associated with GHG-induced warming as typically projected for the end of the 21st century [*Wang et al*., 2012]. Although our results will undoubtedly differ in quantitative detail from what a more comprehensive model would yield, the idealized model should be adequate for capturing qualitative climate changes in tropospheric transport while illustrating how air-mass fractions quantify such changes.

3.2. Idealized REF and FTR Circulations

[22] Figure 2a shows the mass stream function of the model's 1000 day climatology, with the dominant Hadley cell in the NH and an intertropical convergence zone (ITCZ) at approximately 7°S, as expected under perpetual NH winter conditions. In the FTR climate, the Hadley cell expands poleward and weakens (Figure 2a, bottom), which is a dynamical response consistent with CMIP3 projections. As shown in Figure 2b, the model's climatology features tropospheric midlatitude jets centered at 40°S and 32°N. These jets shift poleward under idealized climate change to approximately 46°S and approximately 36°N (Figure 2b, bottom). The associated eddy kinetic energy per unit mass (EKE, Figure 2c) shifts poleward with the jets.

[23] To aid with the interpretation of the idealized climate changes in the air-mass fractions, it is useful to highlight additional key changes in the circulation. To that end, Figure 3 shows the changes in the residual-mean downwelling at the tropopause, in the EKE, and in the isentropic structure of the troposphere. Figure 3a shows the residual-mean vertical velocity $\bar{w}^*$ at the tropopause, and Figure 3b shows its climate change $\Delta\bar{w}^*$, as a function of latitude. There is reduced downwelling at approximately 60° latitude and slightly increased downwelling at midlatitudes in both hemispheres.

[24] Figure 3c shows the contours of the FTR-REF difference ΔEKE superposed on the tropopause and selected isentropes of the REF and FTR climates. The dipolar pattern of ΔEKE in each hemisphere is located approximately at the

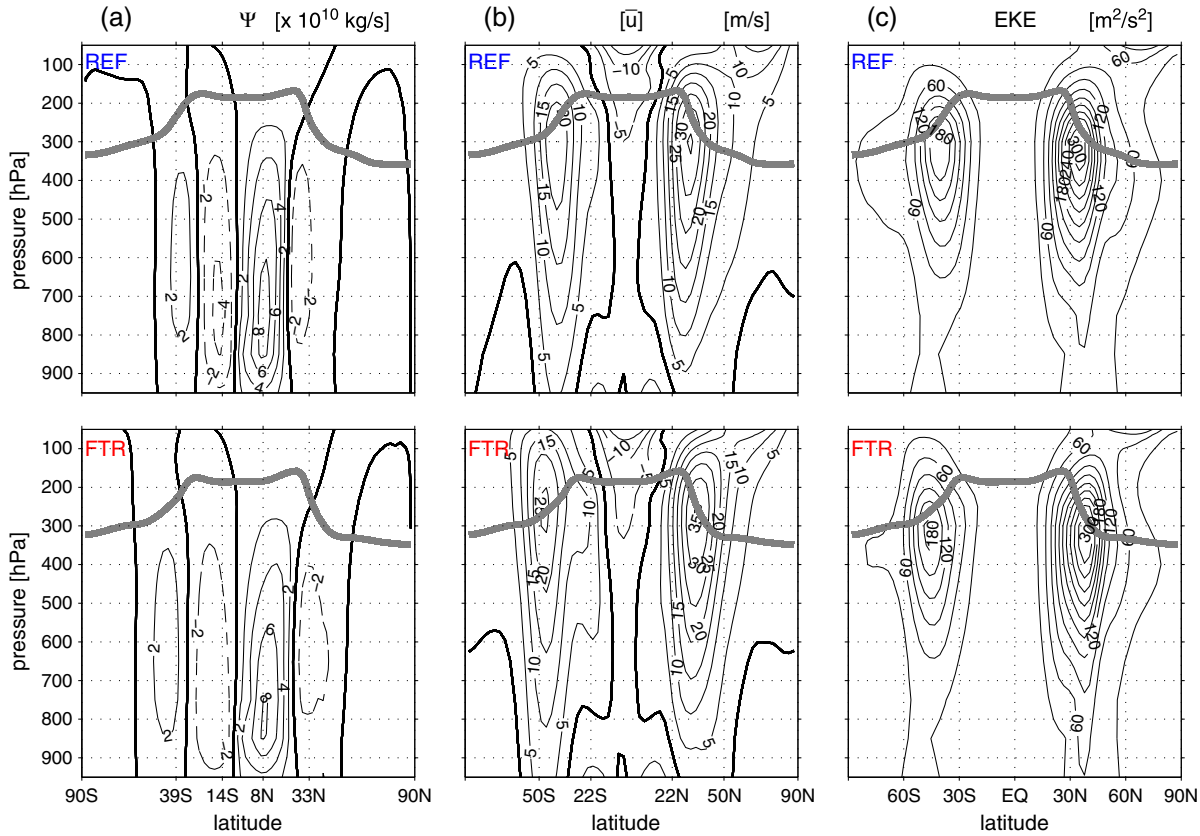

Figure 2. (a) The Eulerian time-mean mass stream function, Ψ, (b) the time and zonal mean zonal winds, $[\bar{u}]$, and (c) the EKE per unit mass, due to both transient and standing eddies, for the REF (top) and FTR (bottom) climates. The time and zonal mean thermal tropopause is indicated by the thick gray line. The contour interval is 2×10^{10} kg s^{-1} for Ψ, 5 m s^{-1} for $[\bar{u}]$, and 30 m^2/s^2 for EKE. Thick black lines are zero contours. For Ψ, latitude ticks mark the PBL origin regions, and for $[\bar{u}]$ they mark the STRAT origin regions.

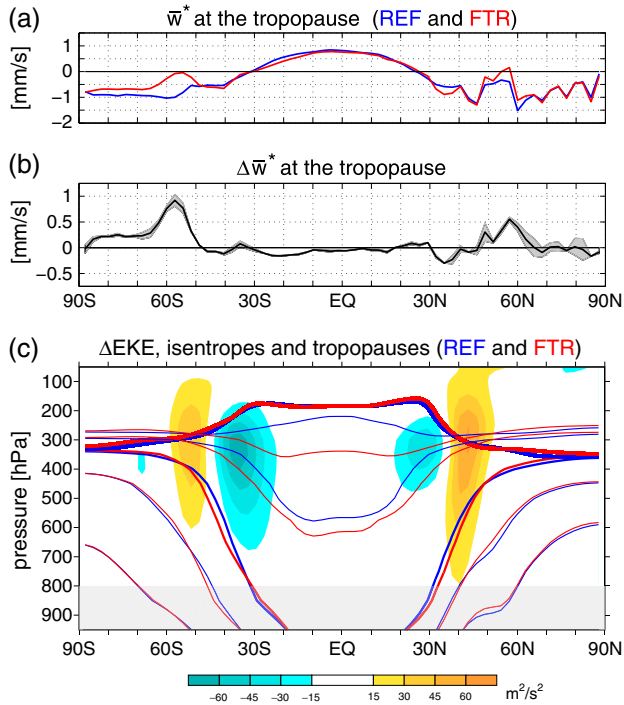

Figure 3. (a) The climatological residual-mean vertical velocity at the tropopause computed as a vertical average of $\bar{w}^*$ using Gaussian weights with a 25 hPa standard deviation centered on the time and zonal mean tropopause. The blue line is for the REF climate, and the red line is for the FTR climate. (b) The corresponding climate change difference $\Delta\bar{w}^*$ and its associated uncertainty (gray shading), estimated as $\pm\left(\delta\bar{w}^*_{\mathrm{REF}} + \delta\bar{w}^*_{\mathrm{FTR}}\right)$. Here, $\delta\bar{w}^* \equiv \left|\bar{w}^*_1 - \bar{w}^*_2\right|/2$ and the subscripts 1 and 2 denote two different 1500 day means. (c) The FTR-REF change in the ΔEKE (filled contours), the climatological tropopauses of the REF and FTR climates (heavy lines), the approximate climatological zonal-mean boundary between the underworld and middleworld (heavy isentropes at 285 K in the SH and at 276 K in the NH), and some additional representative isentropes (265 K and 275 K in the SH underworld, 255 K and 265 K in the NH underworld, and 295 K and 302 K in the middleworld). The gray-shaded region indicates our idealized PBL where the Rayleigh friction acts.

jet latitude and indicates a polarward shift of the EKE. Interestingly, the positive ΔEKE anomaly in the NH extends toward the surface with important implications for the PBL air-mass fractions, as described in the following sections. The equatorward negative ΔEKE anomaly in the NH is localized in the upper troposphere. In the Southern Hemisphere (SH), both positive and negative ΔEKE anomalies extend through most of the free troposphere. Although some extension of the EKE toward the surface can be seen in the climate change response of comprehensive models, this surface intensification of the eddies is likely exaggerated in our idealized model [*Lorenz and DeWeaver*, 2007].

[25] The REF and FTR mean tropopauses in Figure 3c show that with our representation of future conditions, the tropopause is lifted at high latitudes relative to its REF position. Closer examination shows that this lift is in the range of 15 to 20 hPa, which is similar to anthropogenically forced tropopause changes in future projections by comprehensive GCMs [*Holzer and Boer*, 2001; *Lorenz and DeWeaver*, 2007]. Figure 3c also shows the isentropes separating the middleworld from the underworld, using the terminology of *Hoskins* [1991]. (The underworld is the region of the atmosphere whose isentropes lie entirely in the troposphere, whereas the middleworld is the region of the atmosphere whose isentropes cross the tropopause.) In the FTR climate, the isentropes separating the middleworlds and underworlds can be seen to have moved poleward in the middle troposphere relative to their REF positions. This expansion of the middleworld is expected from the warming of the model's midlatitude and upper tropical troposphere. We emphasize that this shift of the isentropes is a large-scale dynamical response to very localized upper tropospheric heating, consistent with poleward-shifted jets in thermal wind balance with poleward-shifted temperature gradients.

3.3. The Diagnostic Tracers

3.3.1. Air-Mass Fractions of Last Boundary Layer Contact

[26] Because the idealized model has no boundary-layer turbulence parameterization, we deem the lowest two model layers (800 hPa to the surface) to be the model's "PBL." This choice is also consistent with the model's Rayleigh drag coefficients, which decrease linearly with $\sigma = p/p_s$ to zero at $\sigma = 0.7$. The PBL is partitioned into the five regions Ω_i shown in Figure 1a. The Ω_i are zonally symmetric strips chosen to straddle the latitudes where the tropospheric overturning circulation transitions from ascent to descent in both the REF and FTR climates (Figure 2a). We use two-letter subscripts to identify the Ω_i regions of the PBL: SU (SH underworld), SS (SH subtropics), EQ (equatorial), NS (NH subtropics), and NU (NH underworld). Note that the SU and NU regions lie well within the underworld (Figure 3); they are not meant to define the surface extent of the underworld. Thus defined, these regions are predominantly associated with either large-scale ascent or descent in both the REF and FTR climates so that their respective air-mass fractions can be compared for similar flow regimes.

[27] We carry five passive PBL (subscript B) air-mass tracers $f_{\mathrm{B}}(\mathbf{r}, t|\Omega_i)$, one for each Ω_i region. After the dynamical variables are spun up to climatology, the f_{B} tracers are introduced and integrated for 5000 days, after which they have equilibrated [equation (3) is satisfied everywhere]. We then calculate the climatological means of f_{B} over a further 3000 days of integration. Because we run in statistically stationary DJF mode, this is equivalent to averaging over approximately 30 boreal winter seasons.

3.3.2. Air-Mass Fractions of Last Stratosphere Contact

[28] We identify the tropopause using the standard WMO definition [*World Meteorological Organization (WMO)*, 1957): the tropopause is located at the lowest model level where the lapse rate decreases to 2 K/km, with no increase for 2 km above that. This thermal tropopause is computed online for each time step and at every horizontal grid point. We partition the stratosphere into five axisymmetric regions Ω_i as shown in Figure 1b. These regions are chosen to be hemispherically symmetric and designed to straddle the midlatitude tropospheric jets in both the REF and FTR climates, so that changes in the corresponding air-mass fractions can be interpreted without worrying about the Ω_i

regions shifting into different flow regimes when the jets shift slightly poleward.

[29] To identify the five Ω_i of the stratosphere we use the subscripts SP (SH high/polar latitudes), SM (SH midlatitudes), TR (tropics), NM (NH midlatitudes), and NP (NH high/polar latitudes). Because the stratospheric air masses f_S only evolve in the troposphere (in the stratosphere their values are held at either zero or unity), we need to integrate only for 3000 days for f_S to reach equilibrium. The climatological means are then evaluated over a further 3000 days of integration.

[30] For both f_B and f_S, we verified that stationary-state fluctuations of a 1500 day mean are about an order of magnitude smaller than the diagnosed climate changes Δf_B and Δf_S. We may therefore rest assured that climate changes in the 3000 day mean air-mass fractions are robustly detected and not obscured by natural variability.

4. Results

[31] The air-mass fractions defined here have characteristic climatological distributions and responses to our idealized global warming that we now examine systematically. For our statistically stationary perpetual DJF flow, it suffices to focus on the time and zonal mean air-mass fractions denoted here simply by $\bar{f}$. Because the air-mass fractions sum to unity at every point [equation (3)], the climate changes $\Delta\bar{f}$ must sum to zero: $\sum_i \Delta\bar{f}(\mathbf{r}|\Omega_i) = 0$. Hence, in terms of the air masses, climate change means a change in the relative proportions of the air masses, with an increase in any single air mass always being compensated by decreases in one or more of the other air masses.

4.1. PBL Air-Mass Fractions

[32] First, we examine the equatorial PBL air-mass fraction, $\bar{f}_B(\mathbf{r}|\Omega_{EQ})$ or simply "Ω_{EQ} air," shown in Figure 4 (third row). The Ω_{EQ} region straddles the ITCZ, a region of low-level convergence and upper-level divergent outflow. Consequently, $\bar{f}_B(\mathbf{r}|\Omega_{EQ})$ is high (>0.5) in the middleworld and overworld, and small throughout the underworld, again using the terminology of *Hoskins* [1991]. The underworld is filled with PBL air of nonequatorial origin (see following paragraphs). A finer contour interval (data not shown) reveals that in the stratosphere, the maximum values lie in the tropics where Ω_{EQ} air enters the stratospheric overworld from the troposphere. The high fractions in the upper midlatitude and high-latitude troposphere are due to exchange with the stratosphere,

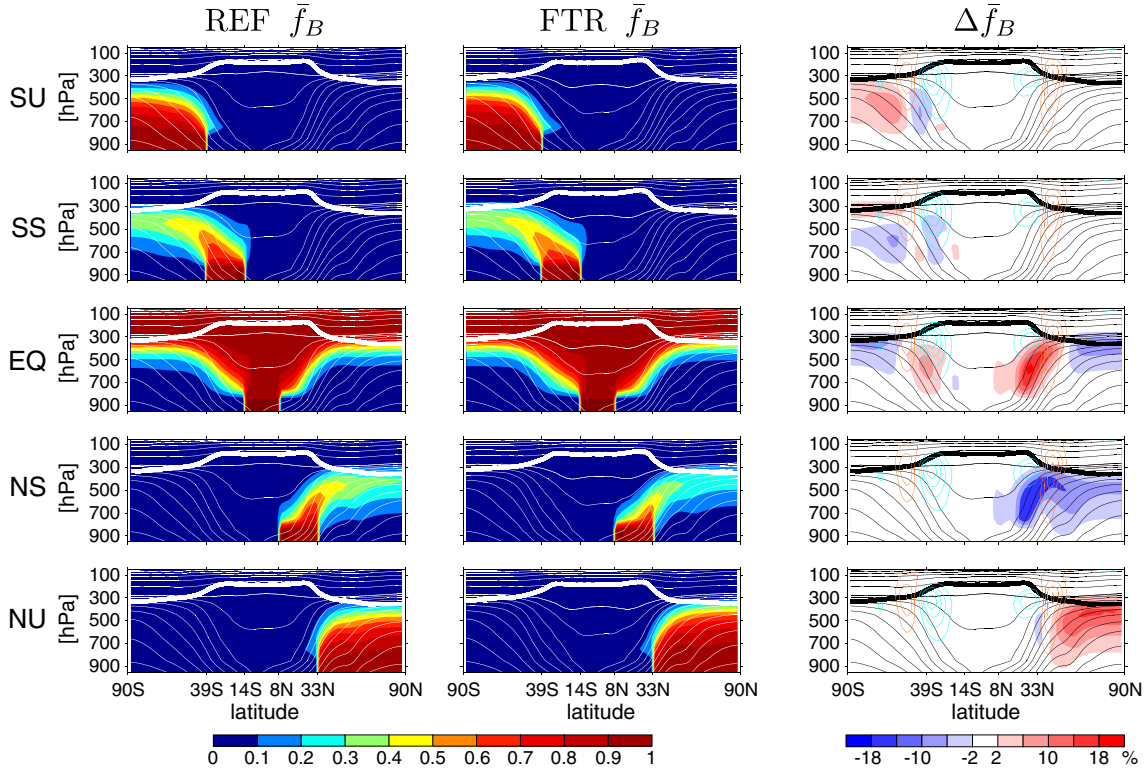

Figure 4. Colored field: the fraction of air that was last at the PBL at the SH underworld (SU, first row), SH subtropics (SS, second row), equatorial region (EQ, third row), NH subtropics (NS, fourth row), and NH underworld (NU, fifth row). Air-mass fractions, $\bar{f}_B(\mathbf{r}|\Omega_i)$, are shown for the REF and FTR climates. Isentropes are overlaid in white (contours every 30 K). The time and zonal mean thermal tropopause is indicated by the thick white line. The FTR-REF changes Δf are shown in the right panel and overlaid with the isentropes (thin lines) and the tropopause (thick black line) of the REF climate. Also superposed are the contours of the changes in eddy kinetic energy (orange contours for $\Delta\mathrm{EKE} \geq 15\ \mathrm{m^2 s^{-2}}$ and cyan contours for $\Delta\mathrm{EKE} \leq -15\ \mathrm{m^2 s^{-2}}$, with a contour interval of $15\ \mathrm{m^2 s^{-2}}$). Latitude ticks mark the bounds of the PBL origin patches.

which is nearly saturated with Ω_{EQ} air (see also section 4.2, in which we examine the effect of eliminating stratospheric pathways from the diagnostic). The Ω_{EQ} air mass represents 61% of the mass of the free troposphere (Table 1).

[33] The FTR-REF climate change difference $\Delta\bar{f}_B(\mathbf{r}|\Omega_{EQ})$ plotted in Figure 4 (right column, third row) reveals positive anomalies that are roughly aligned with the isentropes at the boundary between the middleworld and underworld. This indicates a poleward expansion of the Ω_{EQ} air mass in response to an expanding tropospheric middleworld (Figure 3). That the poleward expansion of the air mass is largest in the NH is expected from the dominant NH Hadley cell in our perpetual DJF regime. Globally integrated, the free tropospheric Ω_{EQ} air mass increases by 3%.

[34] In addition to positive anomalies, $\Delta\bar{f}_B(\mathbf{r}|\Omega_{EQ})$ has smaller negative anomalies localized at high latitudes just under the tropopause and extending to the mid-troposphere. The reduced Ω_{EQ} air at these locations in the FTR climate corresponds to a first-order upward shift of the $\bar{f}_B(\mathbf{r}|\Omega_{EQ})$ vertical profile by approximately 20 hPa and is therefore most likely a consequence of the high-latitude lift of the tropopause.

[35] Consider now the NH subtropical Ω_{NS} air-mass fraction (Figure 4, fourth row), which represents 10% of the mass of the free troposphere (Table 1). The Ω_{NS} origin region straddles isentropes from both the middleworld and underworld. The plume of the Ω_{NS} air mass extends to the tropopause and is broadly aligned with the isentropes, underlining the predominantly adiabatic transport. Poleward from the source region, the Ω_{NS} plume is diluted as it mixes with PBL air from elsewhere. The Ω_{NS} air mass responds to changes in the mean state by "getting out of the way" of the expanding equatorial air mass and also to changes in the midlatitude eddies, as we now examine further.

[36] Comparing the Ω_{NS} plumes for the FTR and REF cases, we see that in the FTR model climate, the plume is of weaker amplitude. This reduced amplitude is at least in part due to less effective escape from the PBL (as opposed to more effective mixing and dilution), as evidenced by a 26% reduction in the global burden of the Ω_{NS} air (Table 1). The climate change $\Delta\bar{f}_B(\mathbf{r}|\Omega_{NS})$ plotted in Figure 4 (right column, fourth row) shows a large negative anomaly where the Ω_{EQ} air mass had a dominant positive anomaly, which means that the same mechanism is at play: the isentropes are shifted poleward, decreasing the Ω_{NS} air above the Ω_{NS} region while increasing the Ω_{EQ} air there.

[37] At higher latitudes, the changes $\Delta\bar{f}_B(\mathbf{r}|\Omega_{NS})$ may be understood in terms of changes in mixing along isentropes by baroclinic waves. To interpret the changes in Ω_{NS} air in terms of changes in stirring and mixing, we overlay the anomaly panels of Figure 4 with contours of ΔEKE (see also Figure 3). As a consequence of the poleward shift of the EKE, eddies in the FTR climate are less effective at mixing PBL air adiabatically away from the subtropical Ω_{NS} region (as already noted previously), but more effective in diluting this air at middle latitudes and high latitudes. In the SH, the subtropical Ω_{SS} air mass undergoes broadly similar changes as the Ω_{NS} air mass, but with much reduced amplitude due to the perpetual DJF regime, which has a stronger warming response in the NH.

[38] Next, we examine the midlatitude and high-latitude Ω_{NU} PBL air-mass fraction (Figure 4, fifth row), which represents 10% of the mass of the free troposphere (Table 1). As the subscript suggests, this air mass is largely confined to the underworld. The plot of $\Delta\bar{f}_B(\mathbf{r}|\Omega_{NU})$ in Figure 4 reveals that the FTR model climate has increased Ω_{NU} air in the upper NH underworld, with a global burden that is 9% larger in the future (Table 1). Based on that fact that the EKE is shifted poleward and intensified toward the Ω_{NU} origin region. Thus, Ω_{NU} air escapes the PBL more successfully, which we attribute to more efficient isentropic stirring and mixing by eddies over the southern edge of the Ω_{NU} origin region as suggested by the fact that the EKE is shifted poleward and surface-intensified toward Ω_{NU}. The additional Ω_{NU} air that escapes the PBL is then transported and mixed isentropically to high latitudes resulting in positive Ω_{NU} anomalies in the upper high-latitude troposphere. Note that this increase in Ω_{NU} air is complementary to the decreases in Ω_{NS} and Ω_{EQ} air in the same region of the troposphere, ensuring that all the $\Delta\bar{f}$ sum to zero. In the SH, a broadly similar increase of Ω_{SU} air in the upper midlatitude and high-latitude troposphere is apparent. The small negative anomaly of Ω_{SU} air over the equatorward edge of Ω_{SU} might be due to weakened EKE there. The globally integrated free-tropospheric Ω_{SU} and Ω_{SS} air masses do not change significantly in the future because their positive and negative anomalies tend to cancel in the integral.

[39] In the stratosphere, the changes for all PBL air-mass fractions are smaller than ± 0.02, and hence, are not visible with the contour interval of Figure 4. A finer contour interval (data not shown) reveals weak negative anomalies of Ω_{EQ} air throughout the entire stratosphere. These negative anomalies are at most 20% as large as the tropospheric anomalies and likely due to a weakening of upper level outflow at the ITCZ (Figure 2a). The negative stratospheric

Table 1. Climatological Mean Fraction of the Global Mass of the Free Troposphere that Was Last in Contact with the PBL at the Origin Regions Indicated

Origin	$\bar{f}_B$ (%)	$\Delta\bar{f}_B$ (%)	$\Delta\bar{f}_B/\bar{f}_B$ (%)	$\bar{f}_B^T$ (%)	$\Delta\bar{f}_B^T$ (%)	$\Delta\bar{f}_B^T/\bar{f}_B^T$ (%)
NU	9.9	0.85	9	9.2	0.49	5
NS	10	−2.6	−26	7.8	−1.4	−18
EQ	61	1.8	3	36	−0.28	−0.8
SS	12	–	–	10	–	–
SU	7.5	–	–	7.4	–	–
$\Sigma\bar{f}$	100	0		70	−1.3	

We consider only the free troposphere (the troposphere excluding the PBL) because the PBL mass fractions are prescribed to either unity or zero in the PBL. Values for the REF climate and the absolute ($\Delta\bar{f}$) and relative ($\Delta\bar{f}/\bar{f}$) FTR-REF climate change are shown. The PBL air-mass fractions are denoted by $\bar{f}_B$, and the troposphere-only PBL fractions, by $\bar{f}_B^T$. A dash indicates that the climate change of the global fraction was on the same order as the natural variability of a 1500 day reference mean and hence not significant.

anomalies of Ω_{EQ} air are largely compensated by weak positive anomalies of subtropical Ω_{SS} air, which are likely due to the following: In the future, Ω_{SS} air in the SH is transported less to the high-latitude troposphere via adiabatic stirring, resulting in negative anomalies there. However, in the future, Ω_{SS} air is nearly as successful in escaping the PBL with a nearly unchanged global burden (Table 1). This means that in the future, more Ω_{SS} air enters the low-level convergence zone of the Hadley circulation, where it is carried into the upper troposphere and entrained into the mean upwelling of the stratosphere. Interestingly, the NH subtropical Ω_{NS} air mass does not display similar anomalies in the stratosphere, possibly because Ω_{NS} straddles the descending branch of the NH Hadley cell such that no significant amounts of Ω_{NS} air enter the ITCZ in either the FTR or REF climates.

4.2. The Troposphere-Only Portion of PBL Air

[40] Here, we ask how much of the PBL air passes through the stratosphere, which is of interest because the photochemical environment of the stratosphere is very different from that of the troposphere and because up to approximately 20% of the interhemispheric surface-to-surface transport has been estimated to pass through the stratosphere [*Holzer*, 2009]. We can straightforwardly determine the fraction of tropospheric PBL air that has never passed through the stratosphere, or equivalently, the fraction that stays strictly in the troposphere denoted by f_B^T, by computing f_B^T exactly like f_B but additionally imposing $f_B^T = 0$ for all points in the stratosphere. Once f_B^T had been computed, the part of f_B that does pass through the stratosphere is then simply determined as the residual $f_B^S = f_B - f_B^T$.

[41] Figure 5 shows the climatological mean decomposition of $\bar{f}_B$ into $\bar{f}_B^T$ and $\bar{f}_B^S$ for the equatorial PBL air-mass fraction (Ω_{EQ}) of the REF climate. The figure demonstrates that essentially all the PBL Ω_{EQ} air mass that can be found in the extratropics, and even in the uppermost tropical troposphere outside the central equatorial region, is either maintained via transport through the stratosphere or is in constant exchange with the stratosphere. The pattern of $\bar{f}_B^S$ shows two plumes of Ω_{EQ} air reaching down toward the surface along the isentropes that cross the tropopause, which highlights the importance of adiabatic stratosphere-troposphere exchange and quantifies the local fraction of Ω_{EQ} air undergoing such exchange. For example, at 500 hPa as much as approximately 35% of the Ω_{EQ} air has passed through the model's stratosphere.

[42] Table 1 shows that approximately 70% of the entire PBL air mass in the free troposphere never reaches the stratosphere, and that approximately half of this air is Ω_{EQ} air. The free tropospheric Ω_{EQ} air mass that never reaches the stratosphere (36% of the total free tropospheric mass) represents just over half the total tropospheric Ω_{EQ} air mass (61% of the total free tropospheric mass; Table 1). The Ω_{NS} and Ω_{SS} air masses reach the stratosphere primarily isentropically, with roughly 20% of their total mass being exchanged with the stratosphere. The Ω_{NU} and Ω_{SU} PBL regions lie well within the underworld outside of the convergence region of the Hadley circulation and are hence largely shielded from the stratosphere.

[43] Table 1 reveals that, in our idealized model, only the NH Ω_{NS} and Ω_{NU} air masses see significant climate changes

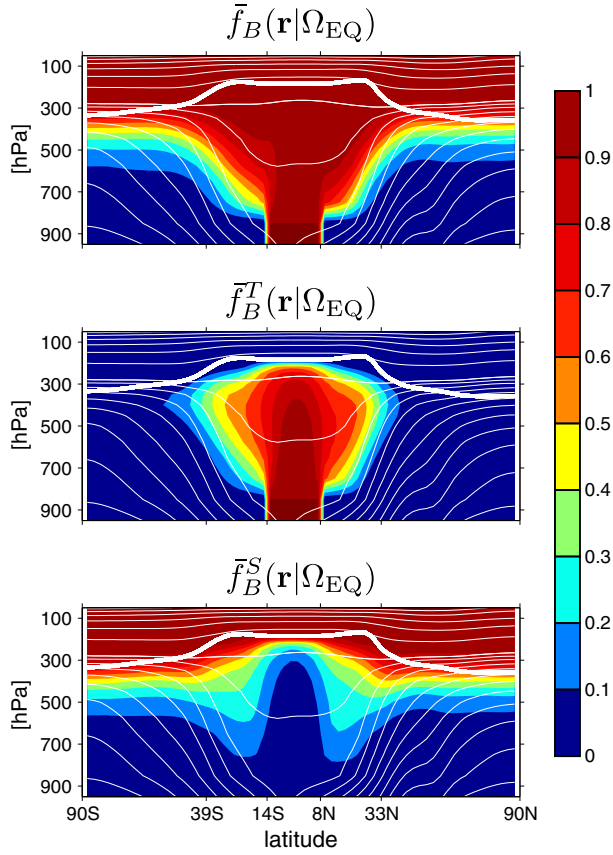

Figure 5. The REF climatology of the partitioning of the Ω_{EQ} PBL air-mass fraction $\bar{f}_B$ (top) into its troposphere-only component $\bar{f}_B^T$ (center) and the component that does visit the stratosphere $\bar{f}_B^S = \bar{f}_B - \bar{f}_B^T$ (bottom). The thick white line indicates the tropopause, and the thin white lines indicate the isentropes (contours every 30 K).

in their tropospheric components. Because these air masses lie mostly in the troposphere to begin with, the relative changes in their troposphere-only components $\Delta\bar{f}_B^T/\bar{f}_B^T$ are similar to the relative changes in the corresponding total free tropospheric air masses $\Delta\bar{f}_B/\bar{f}_B$, although reduced in magnitude because of the missing component that does exchange with the stratosphere.

4.3. STRAT Air-Mass Fractions

[44] We now examine where air in the troposphere was last in contact with the stratosphere. We begin by focusing on Ω_{TR} air defined to have had last tropopause contact in the tropics (Figure 6, middle row). To a first approximation, Ω_{TR} air does not contribute significantly to the troposphere, with a global burden that is less than 4% of the mass of the free troposphere (Table 2). This is expected from the fact that the tropics are a region of mean upwelling across the tropopause (see also Figure 3). Nevertheless, there is some diffusive leakage into the upper troposphere in the presence of very high vertical gradients. Because this diffusion is purely numerical in our model, this small effect is likely not a robustly modeled feature of the atmosphere. The highly localized negative anomaly of $\Delta\bar{f}_S(\mathbf{r}|\Omega_{TR})$ (Figure 6, right column) may be due to a slight uplifting of the tropopause there (and

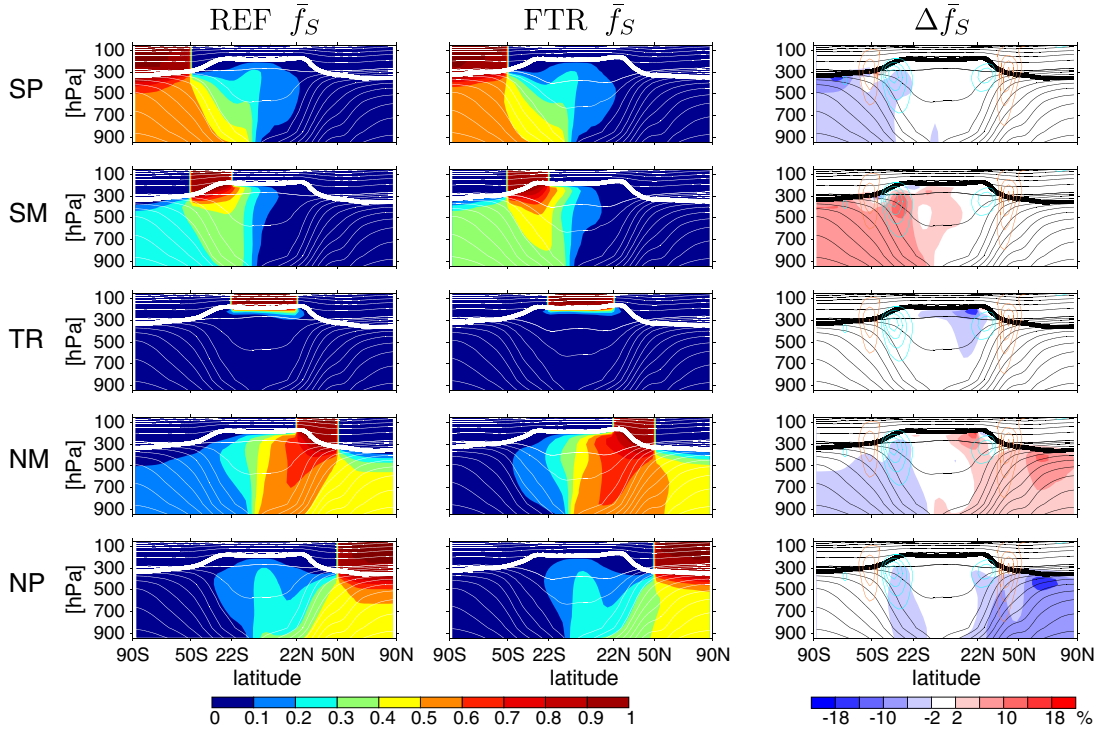

Figure 6. As Figure 3 but for air that was last at the tropopause at the SH high latitudes (SP, top row), SH midlatitudes (SM, second row), tropics (TR, middle row), NH midlatitudes (NM, fourth row), and NH high latitudes (NP, bottom row). Latitude ticks mark the bounds of the STRAT origin patches.

Table 2. Climatological Mean Fraction $\bar{f}_S$ of the Global Mass of the Troposphere (Including the PBL) That Was Last in Contact With the Stratosphere at the Tropopause Origin Regions Indicated

Origin	$\bar{f}_S$ (%)	$\Delta\bar{f}_S$ (%)	$\Delta\bar{f}_S/\bar{f}_S$ (%)
NP	20	−2.5	−13
NM	36	0.78	2
TR	3.8	−1.1	−29
SM	19	3.5	19
SP	21	−0.7	−3
$\Sigma\bar{f}$	100	0	

Values for the REF climate and the absolute ($\Delta\bar{f}_S$) and relative ($\Delta\bar{f}_S/\bar{f}_S$) FTR-REF climate change are shown.

possibly a slight increase in upwelling; Figure 3), in combination with a weakened Hadley cell entraining less of what little Ω_{TR} air does make it into the troposphere.

[45] Air of midlatitude stratospheric origin (Figure 6, second and fourth rows) makes a much more significant contribution to the troposphere: the Ω_{SM} and Ω_{NM} air masses account for 19% and 36% of the global tropospheric mass, respectively (Table 2). These air masses are efficiently transported isentropically into the upper troposphere where they are entrained into the downwelling branch of the Hadley cell. The Ω_{SM} and Ω_{NM} air then enters the ITCZ, ascends, and is detrained aloft into both hemispheres. In the source hemisphere, these air masses spread from the main plume to high latitudes through isentropic mixing. The interhemispheric transport of Ω_{SM} air is much weaker than for Ω_{NM} air because of a weaker SH Hadley cell in our perpetual DJF circulation.

[46] The climate change anomalies for the Ω_{SM} and Ω_{NM} air masses (Figure 6) are positive in the source hemisphere and slightly negative in the opposite hemisphere. (The negative anomalies of Ω_{SM} air in the NH are not visible with the contour interval of Figure 6.) The positive anomalies in the source hemisphere are due to a combination of increased isentropic stirring and mixing across the tropopause and moderately increased mean downwelling across the midlatitude tropopause (Figure 3b). The former is indicated by the positive anomalies of ΔEKE that are centered on the tropopause roughly within the Ω_{SM} and Ω_{NM} geographic regions. (The Ω_{SM} region also straddles the negative ΔEKE anomalies on the equatorward flanks of the jet, but these are mostly located within the interior of the troposphere.)

[47] The increases in the Ω_{SM} and Ω_{NM} air-mass fractions extend to the surface, where they correspond to relative increases of $\Delta\bar{f}_S/\bar{f}_S \simeq$ 25% to 30% for Ω_{SM} and 5% to 15% for Ω_{NM}. The greater change for Ω_{SM} air is in part due to the fact that the interhemispheric transport of the Ω_{SM} air mass is weaker than that of the Ω_{NM} air mass for our hemispherically asymmetric perpetual DJF flow. Thus, increased amounts of Ω_{SM} air will tend to stay in the SH. The increases of Ω_{SM} air in the SH are compensated by decreases in Ω_{NM} air due to decreased interhemispheric transport, and by decreases in Ω_{SP} air, which are discussed below. The localized positive anomaly of Ω_{NM} air in the upper troposphere at approximately 65°N is likely caused by reduced dilution with high-latitude stratospheric air due to decreased downwelling across the tropopause in this region. This decreased downwelling is reflected in weakened negative $\bar{w}^*$ in the future, as seen in Figure 3 (the positive $\Delta\bar{w}^*$ anomaly at ~60°N). The fact that the maximum positive

anomaly of Ω_{NM} air occurs slightly poleward of the maximum $\Delta\bar{w}^*$ reflects the fact that the air-mass changes are not solely governed by changes in the residual mean circulation but importantly also by changes in the quasi-horizontal eddy diffusion.

[48] The negative Ω_{SM} and Ω_{NM} anomalies in the non–source hemisphere are due to reduced interhemispheric exchange, a consequence of a weakened Hadley circulation. On a global average, there is greater cancellation between positive and negative anomalies for the Ω_{NM} air mass than for the Ω_{SM} air mass, with relative changes of 2% versus 19%, respectively (Table 2). The localized positive anomaly of $\Delta\bar{f}_S(\mathbf{r}|\Omega_{NM})$ in the upper tropical troposphere is also associated with a weakened Hadley circulation and complements the negative anomaly of the Ω_{TR} air, ensuring that $\sum_i \Delta\bar{f}_S(\mathbf{r}|\Omega_i) = 0$.

[49] Lastly, we consider the high-latitude Ω_{NP} and Ω_{SP} air masses. These air masses are controlled by mean downwelling at the tropopause and contribute about as much to the mass of the troposphere as the midlatitude Ω_{SM} and Ω_{NM} air masses (~20% each, Table 2). Some of this air is transported isentropically to low latitudes where it is entrained into the ITCZ and detrained aloft into the non–source hemisphere. The dominant anomalies are located in the source hemisphere and negative (Figure 6, right) underlining that the Ω_{NP} and Ω_{SP} air-mass fractions are controlled by downwelling at the tropopause that weakens in the future (Figure 3). The negative anomaly visible for Ω_{NP} in the SH again points to decreased interhemispheric transport.

[50] The anomalies of the Ω_{SP} air mass are weaker than those of the Ω_{NP} air mass despite a greater reduction in mean downwelling across the high-latitude tropopause in the SH than in the NH (Figure 3). This is possibly due to compensation by increased isentropic transport as indicated by positive ΔEKE anomalies that extend into the Ω_{SP} region. In terms of the globally integrated air mass, this manifests itself as a -3% relative change for Ω_{SP} compared with a -13% relative change for Ω_{NP} (Table 2).

5. Discussion

[51] The air masses defined and computed here quantify tropospheric transport in a tracer-independent manner and provide an easily computed metric for assessing climatic changes in constituent transport. Unlike the usual basic flow diagnostics (mean winds, stream functions, mean eddy diffusivities, and the like), changes in the air-mass fractions represent changes in the integrated effect of advection and diffusion and their interactions with the boundary conditions. Although the climate changes in the air-mass fractions, Δf, can be interpreted, as we have done here, in terms of changes in basic circulation diagnostics, we stress that we could not have deduced the patterns of Δf, let alone its quantitative magnitudes, without explicitly computing the air-mass fractions.

[52] When interpreting air-mass fractions, one must keep their physical definitions firmly in mind. For example, the fact that our extratropical PBL air masses do not show significant interhemispheric transport does not indicate a lack of interhemispheric transport, but instead comes from the fact that the PBL air-mass fractions, by construction, track air since last PBL contact. As midlatitude PBL air undergoes interhemispheric transport, it does so through low-level paths into the ITCZ and thus becomes relabeled as subtropical and tropical PBL air along the way. In this sense, the interhemispheric transport of midlatitude PBL air masses is not captured by our PBL air-mass fractions because their PBL identity is prescribed at low levels. However, the interhemispheric transport of the equatorial PBL air mass is captured because it occurs through upper level detrainment from the Hadley cell so that the relabeling in the PBL is not an issue. Similarly, because our STRAT air masses are not reset in the PBL, they also capture interhemispheric transport as seen in Figure 6. Note that if one is interested in the interhemispheric transport of air from the midlatitude PBL, one is at liberty to define air masses differently. For example, one could have extratropical PBL regions in each hemisphere, with a zero-flux surface boundary condition at low latitudes. This would partition air into NH and SH extratropical PBL fractions and capture the interhemispheric transport of these air masses [e.g., *Holzer*, 2009]. It is also worth pointing out that in the formulation of this paper, all air is either of PBL or STRAT origin. If one combines the STRAT and PBL origin patches used here into a single boundary region, the corresponding air-mass fractions would partition tropospheric air simultaneously into fractions of both last PBL and last STRAT contact. Not all air would be of either PBL or STRAT origin, and the fractions would sum to unity only if the sum extends over both the PBL and STRAT patches.

[53] It is perhaps worth noting that the weakened downwelling at high latitudes is opposite to the accelerated Brewer-Dobson circulation (BDC) in the interior of the stratosphere [*Wang et al.*, 2012]. A stronger BDC would lead one naively to expect increased high-latitude stratosphere-to-troposphere transport. However, because the STRAT air masses, as defined here, are held fixed at unity or zero in the stratosphere, they are immune to transport changes in the interior of the stratosphere and only respond to circulation changes in the vicinity of the tropopause. It is important to note that, unlike the STRAT air-mass fractions defined here, chemical tracers with interior sources and sinks such as ozone might develop stronger vertical gradients in the lowermost stratosphere in response to an increased BDC, and hence exhibit increased net flux into the high-latitude troposphere despite decreased residual mean downwelling at the tropopause. We emphasize, therefore, that our STRAT air-mass diagnostic is not designed to capture the response due to interior changes in the stratosphere; instead, our diagnostic captures changes in the tropospheric transport of air that is labeled at the tropopause. Interestingly, the Ω_{EQ} PBL air-mass fractions do not respond to changes of the interior BDC, but to changes in $\bar{w}^*$ at the tropopause because the stratosphere is nearly saturated with Ω_{EQ} air ($\bar{f}(\mathbf{r}|\Omega_{EQ}) \sim 1$) in statistically stationary state.

6. Conclusions

[54] We introduced air-mass fractions that label where air was last in the PBL, or where air was last in contact with the stratosphere (the STRAT fractions), as a diagnostic of tropospheric transport. To illustrate the utility of these air-mass fractions for quantifying climate changes in tropospheric transport, we computed them with an idealized GCM (a

dynamical core). Two statistically stationary, perpetual DJF model climates were compared, one representing an idealized current climate (the REF case) and the other (the FTR case) with a prescribed heating in the upper tropical troposphere resulting in a dynamical response typical of end-of-century projections by comprehensive GCMs. These idealized model climates allowed us to illustrate the nature of our mass fraction diagnostic with the considerable advantage of avoiding the complexities associated with comprehensive GCMs.

[55] For our idealized atmosphere, the PBL air-mass fractions revealed the following changes in the transport climate in response to specified heating in the upper tropical troposphere:

1. The NH midlatitude and high-latitude PBL air-mass fraction increases in the high-latitude upper troposphere, with a 9% relative increase in its global free troposphere burden. This is likely due to poleward-shifted and surface-intensified EKE stirring air more efficiently out of the midlatitude boundary layer. Correspondingly, there is less effective isentropic stirring and mixing of subtropical PBL air away from the source region and enhanced mixing and dilution of that air at midlatitudes.
2. The meridional expansion of the tropospheric middleworld leads to an expansion of the equatorial PBL air mass to higher latitudes and a corresponding contraction of the subtropical PBL air mass. The global free troposphere burden of the NH subtropical PBL air decreases by 26%.

[56] We also computed tropospheric air-mass fractions that label air according to where last contact with the stratosphere occurred. Our key findings for the response of the STRAT air masses are:

1. The midlatitude STRAT fractions increase down to the surface in the origin hemisphere, with particularly large relative changes of approximately 25% at the SH surface. These increases are likely due to increased isentropic eddy transport, and possibly some increased mean downwelling, across the midlatitude tropopause.
2. The high-latitude STRAT air masses decrease in response to decreased downwelling across the high-latitude tropopause. The decreased downwelling brings less high-latitude stratospheric air into the troposphere leading to the less diluted, and hence increased, midlatitude fractions.
3. A weakened Hadley circulation leads to decreased interhemispheric transport through the troposphere.

[57] In addition to being interesting in their own right, the changes in air-mass fractions quantified for our idealized warming have a number of broader implications to the extent that they will be realized in the Earth's future climate. For example, increased NH midlatitude and high-latitude PBL air masses over the wintertime Arctic "cold dome" suggest that, in the future, there may be more transport of black carbon and pollutants such as polychlorinated biphenyl from industrialized regions to the upper Arctic troposphere, where dry deposition (a process not included in this study) could bring them to the surface. This in turn has implications for albedo changes [e.g., black carbon, *Koch and Hansen*, 2005; *Huang et al*., 2010] and biosphere health [e.g., polychlorinated biphenyls, *Malanichev et al*., 2004]. Similarly, the changes in the air masses of last stratosphere contact have implications for the tropospheric distribution of ozone [e.g., *Liang et al*., 2009] and cosmogenic tracers such as beryllium-7 [e.g., *Dibb et al*., 2003; *Liu et al*., 2004], and for the maintenance of the tropospheric moisture budget [e.g., *Waugh*, 2005]. In particular, increases in the air-mass fraction of last contact with the midlatitude tropopause, where most stratosphere-to-troposphere transport takes place, imply potentially increased surface ozone of stratospheric origin (assuming no changes in chemistry), increases in beryllium-7, and drier air.

[58] Our use of an idealized model of course limits the value of our detailed quantitative findings. In particular, the lack of a seasonal cycle might change some of the qualitative features of the air-mass fractions and the relatively coarse resolution may obscure some processes in the upper troposphere/lower stratosphere. The absence of moisture, convection, and boundary-layer turbulence is another key limitation for realistic tracer transport. However, we believe that our qualitative results are relevant to the large-scale NH wintertime flow. We used an idealized model here to illustrate the quantitative utility of air-mass fractions while avoiding the complexities of a comprehensive model such as seasonality and realistic topography. However, we emphasize that air-mass fractions can just as easily be computed with comprehensive models. With a realistic representation of topography and moist thermodynamics, one would want to label PBL air-mass origin based not just on latitude, but also on whether air came from the continental or marine boundary layer, bearing in mind that the detailed climate change responses depends on the location of the region of origin with respect to the circulation features. In future work with comprehensive climate models, we will also include a label that identifies the phase of the seasonal cycle.

[59] Finally, it is important to note that the air-mass fractions defined here are a fundamental aspect of atmospheric transport that captures the boundary-origin information of the boundary propagator, thus complementing the transit time information provided by TTDs (age spectra) and mean age. Air-mass fractions can therefore be computed not only with transport models (for which they would provide a useful model-intercomparison diagnostic), but also estimated from observational tracer data. This has already been demonstrated for the oceans using simple mixing-matrix [e.g., *Tomczak*, 1981] as well as maximum-entropy approaches [*Khatiwala et al*., 2009; *Holzer et al*., 2010; *Holzer and Primeau*, 2010; *Khatiwala et al*., 2012]. Extending these inversion techniques to nonsteady, turbulent atmospheric flow in order to estimate not only mean age but also boundary layer and stratospheric origin is left for future research.

[60] **Acknowledgments.** This work was supported by a NSF grant ATM-0854711.

References

Dibb, J., R. Talbot, E. Scheuer, G. Seid, L. DeBell, B. Lefer, and B. Ridley (2003), Stratospheric influence on the northern North American free troposphere during TOPSE: ^{7}Be as a stratospheric tracer, *J. Geophys. Res.*, *108*, doi:10.1029/2001JD001347.

Gerber, E., and L. Polvani (2009), Stratosphere-troposphere coupling in a relatively simple AGCM: the importance of stratospheric variability, *J. Climate*, *22*, 1920–1933, doi:10.1175.

Haine, T., and T. Hall (2002), A generalized transport theory: water-mass composition and age, *J. Phys. Oceanog.*, *32*, 1932–1946, doi:10.1175/1520-0485.

Hall, T. M., and R. A. Plumb (1994), Age as a diagnostic of stratospheric transport, *J. Geophys. Res.*, *99*, 1259–1070.

Held, I., and M. J. Suarez (1994), A proposal for the intercomparison of the dynamical cores of atmospheric general circulation models, *Bull. Am. Meteor. Soc.*, *75*, 1825–1830.

Holzer, M. (2009), The path density of interhemispheric surface-to-surface transport. Part II: Transport through the troposphere and stratosphere diagnosed from NCEP data, *J. Atmos. Sci.*, *66*, 2172–2189, doi:10.1175/2009JAS2895.1.

Holzer, M., and G. J. Boer (2001), Simulated changes in transport climate, *J. Climate*, *14*, 4398–4420.

Holzer, M., and T. M. Hall (2000), Transit-time and tracer-age distributions in geophysical flows, *J. Atmos. Sci.*, *57*, 3539–3558, doi:10.1175/1520-0469.

Holzer, M., and F. Primeau (2010), Improved constraints on transit time distributions from argon 39: A maximum entropy approach, *J. Geophys. Res.*, *115*, C12021, doi:10.1029/2010JC006410.

Holzer, M., F. Primeau, W. Smethie Jr., and S. Khatiwala (2010), Where and how long ago was water in the western north atlantic ventilated? Maximum-entropy inversions of bottle data from WOCE line A20, *J. Geophys. Res.*, *115*, doi:10.1029/2009JC005750.

Hoskins, B. J. (1991), Towards a PV-Theta view of the general circulation, *Tellus*, *43*, 27–35.

Huang, L., S. L. Gong, S. Sharma, D. Lavoue, and C. Q. Jia (2010), A trajectory analysis of atmospheric transport of black carbon aerosols to Canadian High Arctic in winter and spring (1990-2005), *Atmos. Chem. Phys.*, *10*, 2221–2244.

Khatiwala, S., F. Primeau, and T. Hall (2009), Reconstruction of the history of anthropogenic CO_2 concentrations in the ocean, *Nature*, *462*, 346–349, doi:10.1038/nature08526.

Khatiwala, S., F. Primeau, and M. Holzer (2012), Ventilation of the deep ocean constrained with tracer observations and implications for radiocarbon estimates of ideal mean age, *Earth Planet Sci. Lett.*, *325–326*, 116–125, doi:10.1016/j.epsl.2012.01.038.

Koch, D., and J. Hansen (2005), Distant origins of Arctic black carbon: A Goddard Institute for Space Studies ModelE experiment, *J. Geophys. Res.*, *110*, D04204, doi:10.1029/2004JD005296.

Langenhorst, A. (2005), Spectral Atmospheric Core Documentation, Geophysical Fluid Dynamics Laboratory, Princeton, NJ.

Liang, Q., A. Douglass, B. Duncan, R. Stolarski, and J. Witte (2009), The governing processes and timescales of stratosphere-to-troposphere transport and its contribution to ozone in the arctic troposphere, *Atmos. Chem. Phys.*, *9*, 3011–3025, doi:10.5194/acp-9-3011-2009.

Lin, S., and R. Rood (1996), Multidimensional flux-form semi-lagrangian transport schemes, *Mon. Weather Rev.*, *124*, 2046–2070, doi:10.1175/1520-0493.

Liu, H., J. Dibb, A. Fiore, and R. Yantosca (2004), Constraints on the sources of tropospheric ozone from Pb-210-Be-7-O3 correlations, *J. Geophys. Res.*, *109*, doi:10.1029/2003JD003988.

Lorenz, D. J., and E. T. DeWeaver (2007), Tropopause height and zonal wind response to global warming in the IPCC scenario integrations, *J. Geophys. Res.*, *112*, D10119, doi:10.1029/2006JD008087.

Malanichev, A., E. Mantseva, V. Shatalov, B. Strukov, and N. Vulykh (2004), Numerical evaluation of the PCBs transport over the Northern Hemisphere, *Environ. Pollut.*, *128*, 279–289, doi:10.1016/j.envpol.2003.08.040.

Meehl, G., C. Covey, T. Delworth, M. Latif, B. McAvaney, J. Mitchell, R. Stouffer, and K. Taylor (2007), The WCRP CMIP3 multimodel dataset - A new era in climate change research, *Bull. Am. Meteor. Soc.*, *88*, doi:10.1175/BAMS-88-9-1383.

Miller, R., G. Schmidt, and D. Shindell (2006), Forced annular variations in the 20th century intergovernmental panel on climate change fourth assessment report models, *J. Geophys. Res.*, *111*, doi:10.1029/2005JD006323.

Polvani, L. M., and P. J. Kushner (2002), Tropospheric response to stratospheric perturbations in a relatively simple general circulation model, *Geophys. Res. Lett.*, *29*(7), doi:10.1029/2001GL014284.

Tomczak, M. (1981), A multi-parameter extension of TS-diagram techniques for the analysis of non-isopycnal mixing, *Prog. Oceanogr.*, *10*, 147–171.

Wang, S., E. Gerber, and L. Polvani (2012), Abrupt circulation responses to tropical upper tropospheric warming in a relatively simple stratosphere-resolving AGCM, *J. Climate*, *25*, 4097–4115, doi:10.1175/JCLI-D-11-00166.1.

Waugh, D. (2005), Impact of potential vorticity intrusions on subtropical upper tropospheric humidity, *J. Geophys. Res.*, *110*, 12,149–12,161, doi:10.1029/2004JD005664.

World Meteorological Organization (WMO) (1957), Meteorology, a three-dimensional science: second session of the commission for aerology, in WMO Bulletin IV(4), WMO, Geneva, Switzerland.

Yin, J. (2005), A consistent poleward shift of the storm tracks in simulations of 21st century climate, *Geophys. Res. Lett.*, *32*, doi:10.1029/023684.